Al-Mustansiriyah Journal of Science
ISSN: 1814-635X (print) 2521-3520 (electronic)

ORIGINAL ARTICLE OPEN ACCESS

A Machine Learning Approach for Identifying Five Types of Horizontal Ocular Disorders Using Haar Features

Bassam AlKindy [a], Oras B. Jamil [a], Huda Al-Nayyef [a], and Wissam Alkendi [b]

[a] Department of Computer Science, College of Science, Mustansiriyah University, Baghdad, Iraq
[b] UTBM, CIAD UR 7533, F-90010 Belfort, France

CORRESPONDENCE
Bassam AlKindy
dr.balkindy@uomustansiriyah.edu.iq

ARTICLE INFO
Received: September 12, 2024
Revised: March 02, 2025
Accepted: March 15, 2025
Published: March 30, 2025

ABSTRACT: ***Background:*** *The proliferation of digital devices, such as smartphones, TVs, tablets, and laptops, has raised concerns about the potential long-term impact on eye health, particularly from blue light emitted by screens. Related studies suggested that prolonged exposure to blue light may contribute to visual impairments or discomfort.* ***Objective:*** *This research introduces an innovative machine learning approach aimed at diagnosing such visual impairments by automatically detecting the iris center in images using a combination of the Haar Cascade Classifier and Circular Hough Transform algorithm.* ***Methods:*** *The proposed methodology has three phases. The first is the development of a diverse facial image dataset from various datasets through three steps: designing an AdaBoost-based cascaded classifier that identifies the face and the region around the eyes; subsequently, iris boundaries are labeled, where an optimized Hough Transform approach determines its center. Further, the model segments the eye into three regions to ascertain the iris position cause for the deviation of eyes. Finally, RBFN is used to classify five classes of eye strabismus with high accuracy on a horizontal axis.* ***Results:*** *The proposed system presents very promising results with an accuracy equal to 97.5%, precision 0.97834, specificity 0.33333, and recall 0.99632 in iris center coordinates extraction of five classes of horizontal strabismus classification. These findings were validated over two different datasets in order to prove the strength of this model in detecting eye disorders under different light and photo scenarios.* ***Conclusions:*** *This method may be acting like a bridge between computer vision and ophthalmology in ocular health assessment and treatment. Further improvements may open further horizons regarding automated eye detection and diagnosis.*

KEYWORDS: *Haar features; Adaboost classifier; Monocular divergent; Exotropia; Esotropia*

INTRODUCTION

Basically, eye detection serves many significant and critical computer vision applications, including face identification, diagnostics in medical fields, and interactions between humans and computers. Most eye detection systems usually did face identification that sometimes requires quality devices like a high-resolution camera. Such systems may provide good performance; their dependence on access to costly hardware restricts such systems' wide availability. In contrast, low-quality cameras, such as most normal web and mobile devices, would require the application of sophisticated techniques of image processing to extract features for the correct localization of iris centers. Therefore, this is the challenge in upscale outreach by eye detection systems in resource-constrained environments [1], [2].

Detection of eyes is a bit more critical, especially in systems analyzing the shape of the mouth or the location of the iris in complicated situations, such as daylight or infrared light. Precise Iris Localization helps researchers understand facial expressions and is a significant concern for medical purposes. For example, one can study the facial variations caused by some specific diseases or infections. While significant research has been carried out in this regard, the existing methods developed

so far experience difficulties due to the presence of different facial expressions, occlusions, and lighting conditions. Low cost but efficient methods for eye detection that can be applied under variable conditions are still highly in demand [3], [4].

The following are some of the questions that this research has tried to address: How will low-resolution cameras be used for the detection and localization of irises in eyes meant for challenging situations? What would be the extent of machine learning and computer vision techniques in surpassing the challenging situations like occlusion and variation of light in detecting the eyes? Finally, can the proposed method reliably detect and classify different types of horizontal strabismus using automated methods?

To realize this, the paper proposes a machine learning-based automated approach to detect eye regions and classify the types of horizontal strabismus. The proposed system detects the facial and eye regions using Haar cascade classifiers and localizes the iris using the Hough transformation. The current systems have some shortcomings, such as being sensitive to environmental conditions and occlusions on the face; therefore, overcoming these limitations could be used to enhance the robustness and applicability of eye detection methods [5], [6].

The paper is organized as follows: The related Studies section reviews the developments and advancements in eye detection methods. The methodology section presents the datasets used and outlines in details the stages of the proposed model, starting from iris localization and detection techniques until the performance metrics. The results section provides the obtained results, while the discussion section analyzes these results, emphasizing the method performance and outcome. Finally, the conclusion section summarizes the key findings, contributions, and future studies.

RELATED WORKS

The field of face, eye, and iris detection is not novel, and significant research has been conducted in this area. Various studies have focused on identifying the boundaries between the face, eyes, and iris. One noteworthy study conducted in [7] proposes a method for detecting eyeballs through a segmentation stage that involves edge extraction, gray projection, and template matching. In [8] their approach utilizes a generalization technique with a projection function to identify the eyes and determine their center. It is important to note that this is just one example of a significant study in the field, and there may be other relevant research works that have contributed to the advancements in face, eye, and iris detection.

The authors of [9] address issues related to negligent driving behavior contributing to vehicle collisions and fatalities. It highlights challenges in real-time driving performance monitoring, including distractions, lighting variations, and occluded eyes. The proposed approach focuses on identifying frames with vision problems, particularly strabismus and occluded eyes, and normalizes them through Histogram equalization. Three parallel convolutional neural networks (CNNs) are employed to extract features from refined regions of interest (ROIs), and Euclidean distances are computed to classify driver gaze zones. The model is validated on the CAVE-DB dataset, demonstrating improved accuracy compared to previous methods.

Meanwhile, the AdaBoost learning algorithm for integrated image processing and concatenated classifiers in a cascade for face detection was introduced by Viola and Jones [10]. However, this strategy has limitations, such as a sluggish learning process and a substantial number of features involved. In [1], an alternative approach was conducted, using the Sobel operator to find edges.

Another study on identifying strabismus considered a children dataset by [11]. The study addresses the importance of strabismus detection due to its global prevalence in ophthalmology. It proposes a multi-feature model utilizing decision-level weighted fusion, effectively improving strabismus detection performance by extracting discriminative features from the deep image and ratio features. The research emphasizes the efficiency of automatic strabismus detection, saving time and resources for patients and practitioners. Future research directions include exploring the type and degree of strabismus, refining diagnostic techniques, experimenting with different feature fusion methods, and establishing a link between strabismus detection and surgical recommendations, with a focus on benefiting children in under-served areas.

In a similar vein, the application of morphological techniques can be used to extract the eyes and identify face regions. A technique based on edge density was created by [12] for the task of identifying eyes in facial images. This strategy makes use of methods including morphological operations, Sobel edge identification, and histogram equalization. However, the study notes that due to size variances, certain photos might not produce satisfactory findings.

The authors in [13] present a deep learning-based approach for automatically detecting and classifying strabismus disorder using Convolutional Neural Networks (CNNs). The system involves two

key stages: initial detection of facial eye segmentation with the Viola-Jones algorithm, followed by iris-based segmentation of the eye area. It was tested on three strabismus datasets using various experiments and classifiers, achieving an impressive accuracy rate of 95.62%. These findings highlight the efficacy of the proposed CNN-driven system for strabismus detection.

In this study, the main objective focuses on detecting five types of horizontal eye strabismus. The model major focuses on identifying precisely the areas of the eyes. Following that, a rigorously trained machine learning algorithm (such as Radial Basis Function Network (RBFN) is used to determine and identify the exact type of the identified strabismus based on iris position regarding pre-defined regions.

METHODS

Dataset

Image acquisition, which requires choosing an established dataset from earlier studies, is the first stage in the extraction of an eye. The selected photographs should have sharp features, the proper resolution, and be in an appropriate format like JPEG. The amount of illumination, the characteristics of the camera, the distance between the camera and the eye, and the surroundings at the time the image was taken can all have an impact on the quality of the image. To make the analysis and testing easier, this research makes use of two dataset components.

The subjects are facing the camera in Case 1, the first dataset used in this investigation, which is sourced from an earlier study. This dataset, IMPA-FACE3D (IF3D), was first developed in 2008 to facilitate research on facial animation and the analysis of facial expressions. It was first introduced by Somasundaram *et al.* [14]. 38 people in total, 22 men and 16 women, mostly between the ages of 20 and 50 years, make up the dataset. Each image in the collection was given RGB-level conversion before being stored in the "JPEG" format at a 640×480 pixel resolution. 534 photos were taken from this collection and processed using our approach. An illustration of sample photos from the IF3D collection is shown in Figures 1a and 1b.

(a) (b) (c) (d)

Figure 1. Sample images of the dataset. (a, b) IF3D dataset. (c, d) Ophthalmologist dataset.

In Case 2, the second dataset used in this study involves taking pictures using a low-resolution webcam, more specifically a webcam from a laptop, in various lighting situations. A medical stand is used for alignment to guarantee constant face angles. The 35cm separation between the camera and the face is fixed. This dataset comprises images from 47 people (34 men and 13 women) in total, spanning ages 6 to 28 that make up the dataset. Each image in the collection is given an RGB-level conversion and is then stored in the "JPEG" format with a resolution of 640×480. Figures 1c and 1d depict the dataset utilized in this instance.

Preprocessing

The general scenario for the suggested approach includes six steps; after loading an image, the first step will be enhancing image quality by adopting two filters, namely the Gaussian and the Median filters. These filters hugely reduce image noise while improving the quality of the image as a whole.

The second step in the procedure involves face region detection through the use of the Haar Cascade method from the Viola-Jones algorithm [10]. This process involves pointing out a rectangle to detect the position of a pair of eyes. The result is the generation of a bounding box which is divided into two different images meant to be used for the right and left eyes. In the subsequent step, the Circular Hough Transform (CHT) needs further application in each of the different images of the eyes.

The process aims at finding the iris region and finding its center, in respect to the key purpose which the research is conducted for. Figure 2 shows the working process of the proposed approach and how different stages progress in detail.

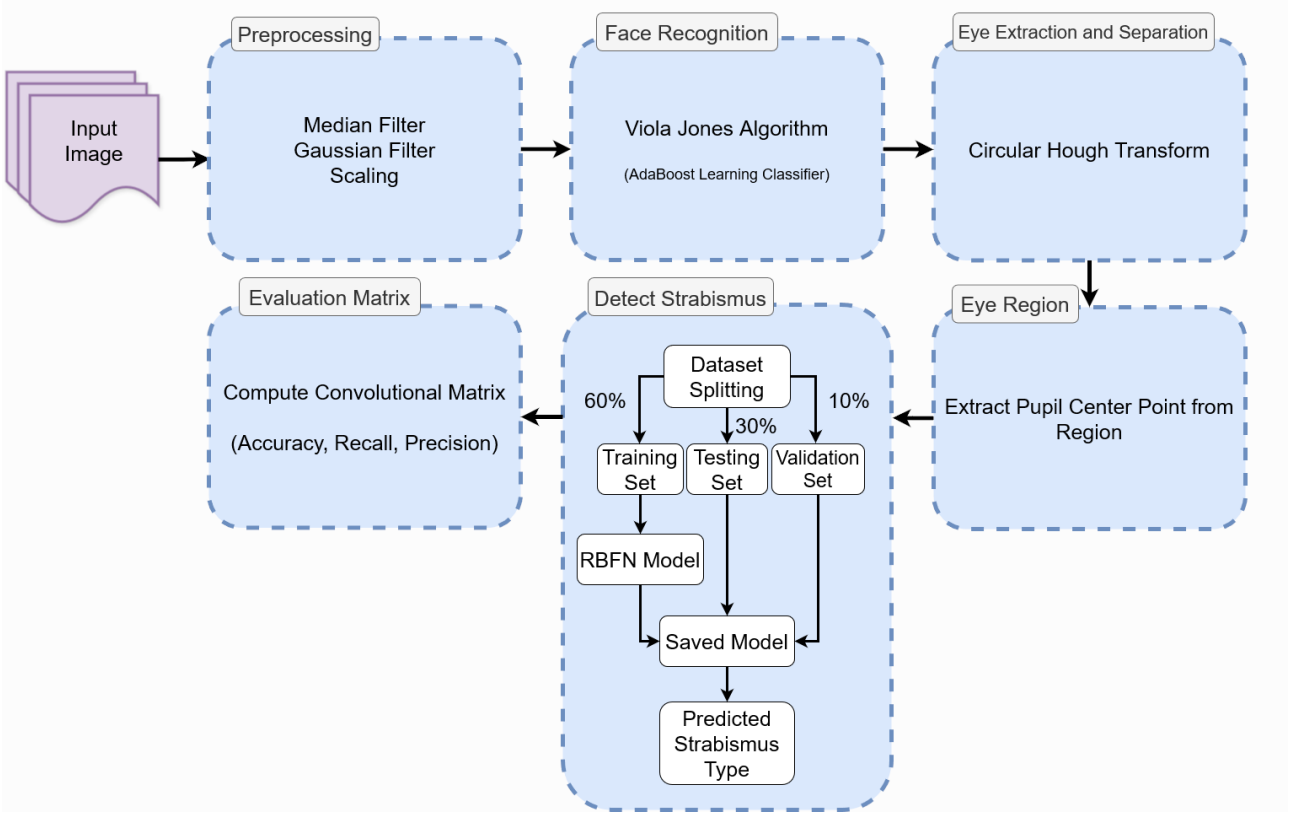

Figure 2. The general pipeline

Image Filtering

The Impa-faced3d (IF3D) dataset images utilized for this project show some degree of noise, which could reduce the efficiency and accuracy of object detection. In this manner, to remove such a problem, a very famous image-processing technique known as noise removal or enhancement is carried out to empower the image by reducing noise; it particularly includes facial and ocular regions. The outcome of such a step is further processed: the converted-to-grayscale enhanced colored image is further processed while maintaining relevant information for the further processing stages to help reduce the computation time.

Maintaining two key requirements is essential when removing noise from a chosen image. First and foremost, the filtered image features must be preserved. Second, the filtered image visual experience must be of the highest caliber. To successfully extract the iris from the facial image and acquire the necessary parameters, a high degree of precision in iris center determination is required. Combining a median filter with a Gaussian filter turns out to be a better option for protecting the edges of the filtered image. With this method, noise reduction is balanced with the preservation of significant image edge details. This set of filters can be used to successfully preserve feature integrity, guarantee aesthetic quality, and safeguard the edges of the image.

The enhancement of the input image to obtain greater accuracy relies heavily on the Gaussian filter, a kind of low-pass filter. It is frequently used for filtering at different levels of image processing. The Gaussian filter significantly enhances image quality, facilitating precise iris recognition in the eye region. The input facial image is effectively smoothed by the application of the Gaussian filter [15], which results in a decrease in model noise. The following formula forms the basis for the filter computation:

$$G(x,y) = \frac{1}{2\pi\sigma^2} e^{-\frac{-x^2+y^2}{2\pi\sigma^2}} \tag{1}$$

where x and y represent the horizontal and vertical axes of the origin and the standard deviation will be fixed to $\sigma = 0.8$ as a proper value, as shown in Figure 3.

(a) Original (b) Gray-scale (c) Gaussian filter (d) Median filter

Figure 3. Enhance dataset images using filters

Correct segmentation of an input image calls for the next step in the process: the application of a median filter. This will allow a photographer to capture finer features of the human subject and accommodate changes in lighting. The Median filter [15] has been one of the most common filters that enhance the contrast and brightness and reduce noise in an image.

Median filter is a nonlinear filter that averages the values of all the pixels of the image with the purpose of smoothing the signal. This number represents the brightness for every output pixel. The median filter is one of the most used smoothing techniques in various digital image processing applications because it can maintain the edges and avoid blurring in the input image [16].

In this work, the application of the median filter enhances the contrast of the image while maintaining the iris margins. Figure 3 shows the application using a kernel size of 3×3 for both rows and columns. This approach maintains the edge of the iris while improving the contrast in the image.

Face Extraction

The detection of the face regions from the filtered image will be done once the image has gone through preprocessing and enhancement stages. It is done by utilizing a trained AdaBoost algorithm based on the Viola-Jones algorithm [10]

The application of this algorithm for extracting the face region serves two primary purposes: reducing the search area and decreasing computational time [16], by accurately identifying the face regions. Subsequent steps can be focused specifically on the facial region of interest, leading to improved efficiency and faster processing.

Identify Eyes using the Haar Feature

Algorithms of pixel-based facial identification frequently have large computational costs. Contrarily, the computing requirements for Haar features, which rely on block features, are typically lower. The calculation efficiency can be raised by utilizing integral pictures. For example, the number of Haar features that may be retrieved from a (24×24) image is up to 16,000 features. As a result, using weak classifiers in conjunction with the AdaBoost method results in a robust classifier [12] for classification while simultaneously easing the computational load.

In face detection systems, Haar features which are derived from the Haar wavelet are crucial elements. As seen in Figure 4, they can be divided into three primary categories. Each category has attributes that are depicted by a template combination of white and black rectangles. These templates' eigenvalues are calculated by deducting the total number of pixels in the white rectangle from the total number of pixels in the black rectangle. The classification of different areas within an image, distinguishing regions with and without faces, is achieved by incorporating 14 feature prototypes as shown in Figure 4. These prototypes consist of 4 edge features, 8 line features, and 2 center-surround features. By independently scaling these prototypes along both the vertical and horizontal directions, a comprehensive and abundant set of features is obtained. This classification method relies on the disparity in eigenvalues between black and white rectangles, as described by [17]. This classification technique leads to the accurate identification of facial features during the upcoming stages of face detection. Notably, the computation of these features remains efficient and consistent, irrespective of their position, as demonstrated by the findings of [18].

Each sample receives a unique set of features as a result of the location, type, and template size variables involved in the extraction of Haar features [19]. Even while each form of Haar feature

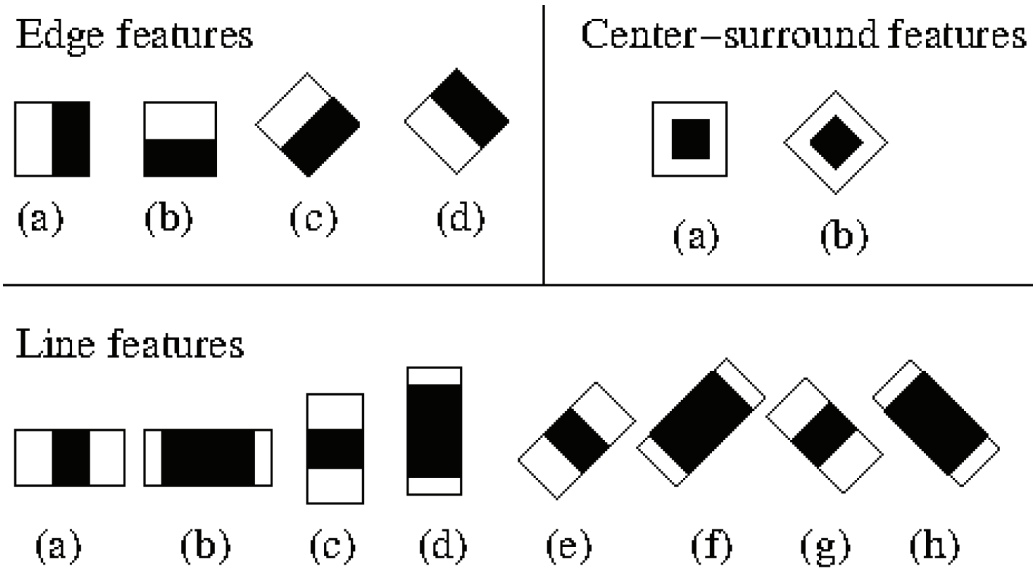

Figure 4. Samples of Haar Feature templates: (a-d) Edge features, (a, b) Center-Surround features, (a-h) Line features.[17]

has a limited ability to discriminate, they all have a distinctive speed. To reach the appropriate detection rate for hierarchical classifiers, hundreds of Haar features are often needed in the later phases of boosting training. The extensive use of features makes up for any potential limitations in the discriminative power of the Haar feature.

It is crucial to employ a strong classifier to ensure a reliable face detection method. One effective approach involves combining weak classifiers with the Adaboost algorithm, such as the Haar cascade classifier based on the Haar feature. It is evident that underperforming classifiers struggle to accurately classify the data. Repeatedly training the weak classifier with different samples is necessary to establish and deploy a system with a resilient classifier. However, this process may be time-consuming and can impact the overall computing speed for detecting eye pair regions. This challenge can be addressed by implementing a hybrid model that integrates various weak classifiers, resulting in robust classifiers that enhance both speed and accuracy [20].

Once the face has been detected, a bounding box (x, y, w, h), as shown in Figure 5, is used to capture the eye pair area based on the Haar features. This approach significantly speeds up the detection of the eye pair region.

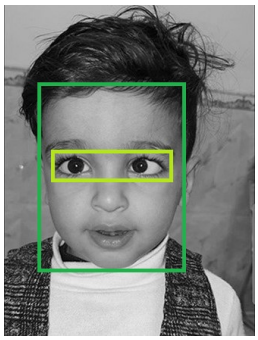

Figure 5. Results from Face and eye identifications.

To capture the eye pair, which is the area of interest in our investigation, the face must be extracted from the acquired image. To identify the eye pair, the Haar feature algorithm, discussed previously in the segmentation phase in face extraction subsection is used, after obtaining the cropped eye pair region. The following step is additional cropping to produce separate images for the left and right eyes. The bounding box derived from the face region is used for this process, as shown in Figure 5. The resulting rectangles, like (x, y, w, h), show where the regions of the identified eye pair have been found. In our method, the center of the nose is used as a benchmark for estimating the region width

and gap between the eyes. As shown in Figure 6, this enables us to produce two eye images.

The Hough transform algorithm is used to set up iris detection. The location of the center of the iris and the radius of the iris are crucial pieces of information that are needed after applying this modification.

(a) (b)

Figure 6. (a) Right eye, (b) Left eye.

Circular Hough Transform to Detect Circle of the Eyes

Hough transform is a method commonly used in pattern detection and description in images, such as line and circle detection [21]. In pattern detection, the first step to consider is the setting of the region of interest, where it characterizes the area in which the pattern detection must take place. Within this area, some parameters are selected to the effect that the target shape is identified. Then, some mathematical expressions translate the transition curve of the original image into points in the region of interest to evaluate the character the target shape has taken. These points are aligned with the characteristic lines and curves of the perceived shape.

The Hough transform gives the search within the region of interest in the chosen parameters by modifications in the curve that has been perceived [22]. When applied to eye recognition, the ocular eye region, which normally manifests itself as a circular component within an input image, is located by the region of interest (ROI) test. The modified Hough transform in isolating the generalized forms relating to the particular shape of interest determines boundaries and extracts iris properties [23].

The Hough transform parametric forms describe the desired function in the detection of circles, lines, and other similar objects. Resistance against picture noise is guaranteed because it gives a flexible space for characterizing the feature boundaries [24]. In addition, it suits locating the circular objects.

Consequently, the Hough transform uses Equation 2 of a circle in the Cartesian coordinate system to detect iris patterns.

$$(x-a)^2 + (y-b)^2 = r^2 \tag{2}$$

where, a and b represent the coordinates of iris centers, and r denotes the radius of the detected iris. It is important to note that the value of r can vary depending on the dimensions of the image. Additionally, (x, y) represents the coordinates of the identified edge point.

Additionally, the radius (r) is randomly selected during trials, taking into account the image size. As depicted in Figure 7, parameters for object polarity and sensitivity were set for the Hough transform, maintaining a constant value of 0.93 across all images. The white line inside the circle within this illustration represents the radius of the two eye regions. In addition, the localized centers of the right eye, denoting iris localization through the Hough transform, are indicated by green markers.

(a) (b)

Figure 7. Iris centers based on regions in (a) Right eye, (b) Left eye

Identify Strabismus from Iris Position

To ascertain the center of the iris within the extracted eye regions, the entire eye is partitioned vertically into three equal sub-regions: the right, center, and left regions, as depicted in Figure 8. The sub-regions are divided into equal segments within the extracted eye region, determined by boundary box, which is derived from the ends and heights of the eye.

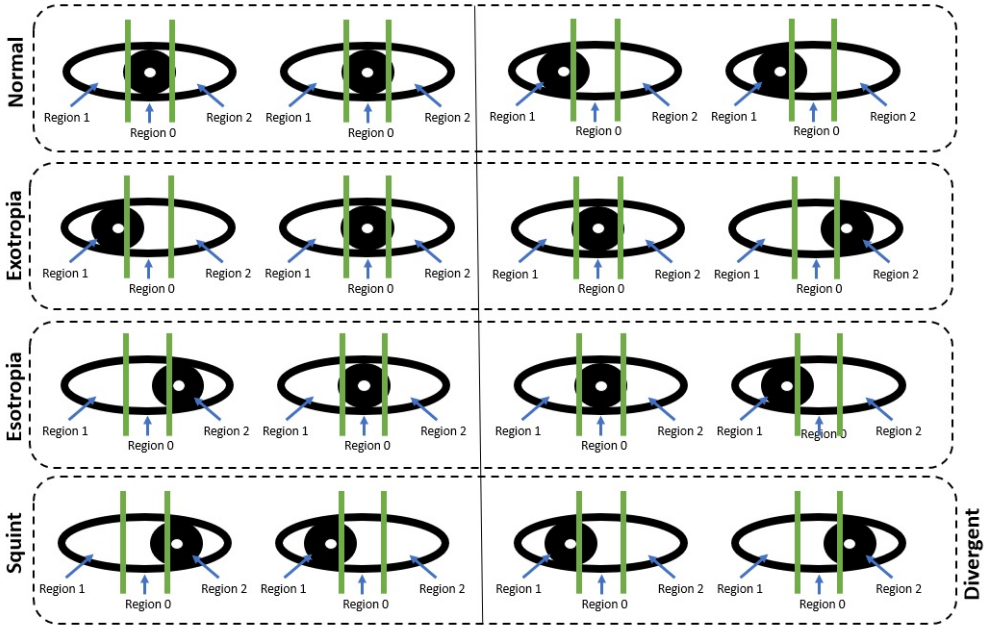

Figure 8. Position of the iris center within the eye region

A standard radial basis function network (RBFN) is then trained to classify the type of strabismus based on the recognized sub-regions of the iris center. The RBFN network is composed of two values input layer, one hidden layer, and 5 bits binary cross-categorical values in output layer (the output will be in the form: 00001: No Strabismus (or Normal), 00010: Esotropia, 00100: Exotropia, 01000: Monocular Divergent, and 10000: Monocular Squint). Furthermore, for the input layer, each sub-region is assigned a corresponding numerical value: 0 for the center, 1 for the right region, and 2 for the left region. This numerical mapping aids in determining the direction and position of the iris center within both the left and right eyes.

By adopting this method, we enable the identification of various types of horizontal eye strabismus, such as Exotropia, Esotropia, Monocular Squint, and Monocular Divergent or normal cases. This is accomplished by comparing the specific regional positions of the central iris point in both the left and right eyes, as illustrated in Table 1.

Table 1. Types of horizontal strabismus cases based on the region position of Iris center

case	IC_L	IC_R	Output class	Strabismus type
1	0	0	1	No Strabismus
2	0	1	2	Esotropia
3	0	2	3	Exotropia
4	1	0	3	Exotropia
5	1	1	1	No Strabismus
6	1	2	4	Monocular Divergent
7	2	0	2	Esotropia
8	2	1	5	Monocular Squint
9	2	2	1	No Strabismus

* IC_L: Iris center in left eye, IC_R: Iris center in right eye.

Vertical-depended strabismus (i.e., hypertropia, hypotropia, and V-shape), falls outside the scope of this study.

Evaluation Metrics

To assess the effectiveness of our proposed method, we utilize three widely used evaluation metrics [25]: Recall (R) or sensitivity, specificity (Sp), accuracy (Acc), and precision (Pr). These metrics can be calculated using the following equations:

$$Recall\ (R) = \frac{TP}{TP + FN}\ , \tag{3}$$

$$Specificity\ (Sp) = \frac{TN}{TN + FP}\ , \tag{4}$$

$$Accuracy\ (Acc) = \frac{TP + TN}{TP + TN + FP + FN}\ , \tag{5}$$

$$Precision\ (Pr) = \frac{TP}{TP + FP}\ , \tag{6}$$

where, TP (true positive), TN (true negative), FP (false positive), and FN (false negative) represent the number of correctly and incorrectly identified images, respectively. The recall (R) and specificity (Sp) metrics measure the algorithm capability to correctly identify images. Accuracy (Acc) is a metric to evaluate the overall classification performance.

RESULTS AND DISCUSSION

The approach revolves around the detection and classification of five horizontal eye strabismus types. The proposed method comprises six stages. Two datasets were employed involving the enhancement of images quality through Gaussian and median filters. The first dataset, IF3D, was previously utilized in a facial emotion detection study by Somasundaram *et al.* [14]. Comprising facial images from 38 individuals, with 14 images per person, the dataset encompasses a total of 532 images. The ages of the individuals range from 20 to 50 years. Within this study, a subset of 113 random images from the IF3D dataset (71 men and 42 women) is selected, represented by the black bars in Figure 9. Notably, the majority of these photographs fall within the 20 to 50 age range. Its important to highlight that while some individuals in this collection have multiple images, others are represented by only one photograph. Variations in environmental capturing conditions likely contribute to this discrepancy.

The second dataset, depicted by white-dashed bars in Figure 9, was employed for this study. It comprises images of 47 individuals (34 men and 13 women) spanning ages 6 to 28. This dataset, obtained from Ophthalmologist sources, underscores its distinctiveness from the IF3D dataset by incorporating age ranges that were previously unrepresented. Notably, it emphasizes images of children aged 6 to 10. Given the extension of the iris radius beyond the eye edge in this age range, the proposed approach must effectively capture the entire iris along with its center.

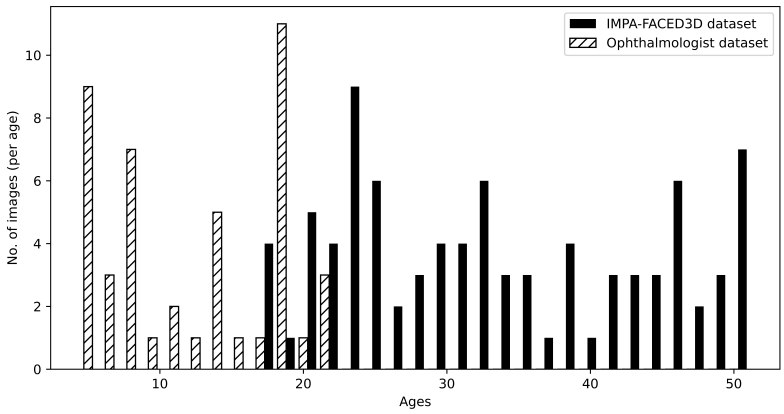

Figure 9. Distribution of two datasets images regarding person age

This dataset also places a particular focus on individuals under the age of 30. The variability in gender, facial expression, illumination, facial angles, and positions within this created dataset adds complexity to iris boundary and fixation point recognition. These two datasets, spanning ages 6 to 50, encompass a diverse array of resolutions, noise levels, and environmental conditions. It is imperative to assess the performance of our method compared to prior research.

Extraction of Eye-pair Region

The method makes use of the Haar Cascade Classifier (HCC) from the Viola-Jones algorithm to pinpoint the location of the eye pair. This algorithm collects Haar features from the chosen facial image, which is then used to locate and center the area containing the eye pair.

It is vital to choose a suitable position for each eye to accomplish adequate centering of the measured region around the eye pair. This is done by creating a range of values that are chosen at random based on the facial region. The bounding box values for the 160 photos in the database used in this study ranged from $[196, 158, 124, 31]$ to $[267, 342, 277, 56]$ at their minimum and maximum values. Various samples from both datasets are shown in Table 2, with the photos with dark backgrounds being from the IMPA-FACED3D dataset while the rest of the images are from Ophthalmologist and Hamid *et al.* [13] datasets as shown in Table 3.

Detection of Iris Region

The Hough transform is used to extract the eye region of interest (i.e., bounding box) from the selected image. The distribution of eye regions for both datasets is shown in Table 2 and Table 3. Within those tables, we present random samples of images sourced from both the IF3D and ophthalmologist datasets. The tables comprise various details, including image name, gender, age, sample number, eye region of interest, iris center coordinates for the right eye, and iris center coordinates for the left eye. The iris features of both eyes are visualized, showcasing their radii and the coordinates of their respective center points. The utilization of the Hough transform facilitates the extraction of the iris area from the images. A depiction of the distribution of eye locations across both datasets is available in Table 2 and Table 3.

The center points, generated from all eye positions, offer insights into the extent of eye deviation when engaged with a screen. Both datasets, comprising around 160 images each resized to dimensions of 640×480 pixels, were processed through the Hough transform, revealing a minimum iris radius of 7.75 pixels and a maximum radius of 14 pixels. It is important to note that the distance between the two eyes is not fixed; this distance is calculated using the Euclidean distance between the locations of the two eye centers. This computation enables us to determine the separation between the centers of the eyes. This distance analysis, based on iris placement, can contribute to the diagnosis of strabismus.

Table 2. Random samples extracted from the IMPA-FACE3D dataset

Image name	Gender	Age	Sample	no	Eye Region of interest (px)				Iris center in Right Eye (px)			Iris center in Left Eye (px)		
					X	Y	Width	Height	Radius	X_R	Y_R	Radius	X_L	Y_L
impa_4_(1)	female	26	4	1	238	220	154	38	9.5	31.47	18.39	9.5	41.88	14.74
impa_4_(2)	female	26	4	2	242	222	158	39	9.75	34.64	19.34	9.75	45.27	15.98
impa_4_(3)	female	26	4	3	247	217	162	40	10	35.70	20.52	10	44.69	21.60
impa_5_(1)	male	34	5	1	215	200	170	42	10.5	32.15	23.71	10.5	49.87	27
impa_5_(2)	male	34	5	2	240	214	178	44	11	34.13	20.36	11	51.58	25.13
impa_5_(3)	male	34	5	3	227	215	171	42	10.5	33.68	20.03	10.5	50.68	25.80
impa_6_(1)	male	34	6	1	236	224	183	45	11.25	35.67	21.09	11.25	49.92	21.86
impa_6_(2)	male	34	6	2	259	182	182	45	11.25	35.52	20.08	11.25	47.96	24.10
impa_7_(1)	female	32	7	1	243	185	186	46	11.5	40.86	21.67	11.5	49.87	21.73
impa_7_(2)	female	32	7	2	253	200	175	43	10.75	39.01	20.27	10.75	46.87	22.45
impa_9_(1)	female	37	9	1	250	203	163	40	10	30.36	18.46	10	47.47	21.73
impa_10_(1)	female	38	10	1	230	195	180	44	11	36.33	22.08	11	51.29	20.68
impa_10_(2)	female	38	10	2	239	169	182	45	11.25	36.67	21.87	11.25	51.26	19.28
impa_11_(1)	male	40	11	1	223	196	186	46	11.5	37.85	18.73	11.5	51.93	21.29
impa_11_(2)	male	40	11	2	210	192	195	48	12	40.02	20.45	12	53.32	25.72
impa_12_(1)	male	44	12	1	240	199	174	43	10.75	38.10	22.99	10.75	49.96	16.22
impa_12_(2)	male	44	12	2	235	202	166	41	10.25	34.56	24.17	10.25	48.14	14.67
impa_13_(1)	male	25	13	1	211	208	165	40	10	36.75	21.15	10	47.21	15.52
impa_14_(1)	male	28	14	1	243	209	164	40	10	32.35	18.40	10	48.84	20.27
impa_15_(1)	male	39	15	1	239	227	182	45	11.25	40.75	18.50	11.25	53.79	21.35
impa_16_(1)	male	30	16	1	233	192	202	50	12.5	46.91	26.81	12.5	58	14.85
impa_16_(2)	male	30	16	2	215	186	191	47	11.75	42.23	25.92	11.75	59.99	12.68
impa_17_(1)	male	35	17	1	243	222	155	38	9.5	33.66	19.14	9.5	42.81	17.2
impa_17_(2)	male	35	17	2	251	213	164	40	10	34.92	18.59	10	45.69	17.31
impa_18_(1)	male	36	18	1	243	210	169	41	10.25	37.34	21.79	10.25	50.03	15.32
impa_19_(1)	female	41	19	1	233	232	162	40	10	35.77	20.74	10	46.15	17.73
impa_19_(2)	female	41	19	2	231	216	174	43	10.75	37.73	21.17	10.75	47.33	18.2

Table 3. Random samples extracted from the Ophthalmologist dataset

Image name	Gender	Age	Sample	no	Eye Region of interest (px)				Iris center in Right Eye (px)			Iris center in Left Eye (px)		
					X	Y	Width	Height	Radius	X_R	Y_R	Radius	X_L	Y_L
Ophth_1_(1)	male	28	1	1	220	293	190	47	11.75	40.16	18.31	11.75	56.12	17
Ophth_1_(2)	male	28	1	2	224	301	186	46	11.5	38.12	11.51	11.5	56.29	15.87
Ophth_1_(3)	male	28	1	3	214	244	193	47	11.75	42.47	20.89	11.75	53.85	23.11
Ophth_2_(1)	male	27	2	1	204	239	209	51	12.75	41.75	21.76	12.75	59.16	30.17
Ophth_3_(1)	male	26	3	1	198	252	218	53	13.25	46.50	30.37	13.25	56.17	24.81
Ophth_3_(10)	male	26	3	10	197	253	218	54	13.5	47.70	28.64	13.5	57.15	23.32
Ophth_4_(1)	male	25	4	1	205	233	212	52	13	50.01	27.08	13	56.07	22.22
Ophth_5_(5)	male	16	5	5	230	297	216	53	13.25	38.03	19.05	13.25	63.21	27.04
Ophth_5_(6)	male	16	5	6	230	296	220	54	13.5	39.30	18.94	13.5	61.79	27.81
Ophth_5_(7)	male	16	5	7	227	294	224	55	13.75	42.11	20.65	13.75	62.79	29.72
Ophth_5_(8)	male	16	5	8	226	293	227	56	14	42.91	21.87	14	61.74	30.99
Ophth_6_(1)	male	17	6	1	228	280	218	54	13.5	40.67	26.33	13.5	65.45	27.29
Ophth_7_(1)	male	12	7	1	210	210	192	47	11.75	45.16	17.58	11.75	61.95	29.31
Ophth_8_(1)	male	11	8	1	218	299	195	48	12	48.64	21.27	12	49.73	79.70
Ophth_8_(2)	male	11	8	2	219	300	192	47	11.75	48.03	26.94	11.75	50.80	69.07
Ophth_9_(1)	male	10	1	1	225	162	187	46	11.5	39.75	19.16	11.5	45.69	28.34
Ophth_10_(1)	male	9	10	1	240	313	175	43	10.75	41.35	20.83	10.75	45.47	24.96
Ophth_11_(1)	male	9	11	1	233	220	217	53	13.25	44.33	15.12	13.25	55.71	21.87
Ophth_11_(2)	male	9	11	2	235	224	212	52	13	41.68	23.74	13	54.81	19.83
Ophth_12_(1)	female	10	12	1	237	336	152	37	9.25	33.82	19.33	9.25	49.43	16.09
Ophth_13_(1)	female	6	13	1	212	337	195	48	12	45.35	22.97	12	52.51	22.51
Ophth_13_(2)	female	6	13	2	215	339	193	47	11.75	44.60	18.75	11.75	50.78	23.29
Ophth_14_(1)	female	7	14	1	232	338	155	38	9.5	34.28	17.85	9.5	45.55	17.14
Ophth_14_(2)	female	7	14	2	248	229	152	37	9.25	30.36	17.03	9.25	43.85	18.41
Ophth_14_(3)	female	7	14	3	247	231	156	38	9.5	30.17	16.33	9.5	41.92	19.23

Predict the Type of Strabismus

In terms of classification, the datasets are divided into 60% training, 30% testing, and 10% validation sets to avoid overfitting. The radial basis function network (RBFN) model is used for classification, with the testing and validation sets representing 40% (281 images). These images are categorized into five groups, each targeting a particular strabismus type, and the results show the predicted strabismus type compared with ground truth values for each image. The research underscores the significance of accurately detecting strabismus types, particularly across diverse age ranges, highlighting the proposed potential approach for improved diagnostics. The categorization of strabismus type hinges on the iris center point position within specific sub-regions, established through the vertical division of the extracted eye regions of interest. By considering the sub-region of the iris center point, the RBFN model is trained to anticipate nine distinct horizontal strabismus classes as illustrated previously in Table 1. A subset of the testing set, consisting of 281 images, is displayed in Table 4, categorized into five groups targeting specific strabismus types.

Table 4. Detection of strabismus from randomly selected test samples using the RBFN model

Sample Label	nb. of images	Image no	dataset	Ground Truth			Strabismus prediction using RBFN		
				Region$_R$	**Region**$_L$	Strabismus type	**Region**$_R$	**Region**$_L$	Prediction Type
11	**111**	1	Opht.	0	0	Normal	0	0	Normal
		2	IMPA.	0	0	Normal	0	0	Normal
		38	IMPA.	0	0	Normal	0	0	Normal
		82	Opht.	0	0	Normal	2	0	Esotropia
		111	IMPA.	0	0	Normal	0	0	Normal
12	**22**	1	Opht.	0	2	Exotropia	0	2	Exotropia
		2	Opht.	0	2	Exotropia	0	2	Exotropia
		8	Opht.	0	2	Exotropia	0	2	Exotropia
		17	Opht.	0	2	Exotropia	0	0	Normal
		22	Opht.	0	2	Exotropia	0	0	Normal
13	**39**	1	Opht.	0	1	Esotropia	0	1	Esotropia
		9	Opht.	0	1	Esotropia	0	1	Esotropia
		18	Opht.	0	1	Esotropia	0	1	Esotropia
		28	Opht.	0	1	Esotropia	0	1	Esotropia
		39	Opht.	0	1	Esotropia	0	0	Normal
21	**74**	1	Opht.	2	0	Esotropia	2	0	Esotropia
		12	IMPA.	2	0	Esotropia	2	0	Esotropia
		29	Opht.	2	0	Esotropia	2	0	Esotropia
		50	Opht.	2	0	Esotropia	2	0	Esotropia
		74	Opht.	2	0	Esotropia	0	0	Normal
31	**35**	1	Opht.	2	0	Esotropia	2	0	Esotropia
		8	Opht.	2	0	Esotropia	2	0	Esotropia
		18	Opht.	2	0	Esotropia	2	0	Esotropia
		27	Opht.	2	0	Esotropia	0	0	Normal
		35	Opht.	2	0	Esotropia	0	0	Normal

Table 4 shows a collection of randomly selected images from the test set, each exhibiting various types of strabismus. These images are subjected to the RBFN training model, which predicts the corresponding strabismus type. The predicted classes are subsequently compared against the actual ground-truth classes.

Model Performance

The accuracy of the model, for each dataset separately, as well as the total performance taking into account both datasets, was calculated using four performance measures. Table 5 displays the results of these performance metrics, which were calculated using Equations (3, 4, 5, and 6).

Table 5. Confusion matrix based on given testing set

Dataset	nb. of Images	TP	TN	FP	FN	Pr	Recall	Sp	Acc
IF3D	160	160	0	0	0	1	1	0	1.0
Other datasets	121	111	3	6	1	0.94872	0.99107	0.33333	0.94215
Total	281	271	3	6	1	0.97834	0.99632	0.33333	0.97509

In Table 5, the Hough transform approach was applied to both datasets, yielding significant results in terms of specificity (0.33333) and Recall (0.99632). This means that even with low-resolution face photos, the suggested method using RBFN model has remarkable detection capabilities in locating the iris border and the center of the eye. The total accuracy achieved by the proposed method is 0.97509. For the high-resolution IF3D dataset, the recognition accuracy reaches 100%, while for the low-resolution dataset, the accuracy is 94.23%.

Comparison with Related Studies

It is critical to realize that the data included in this study includes pictures with different degrees of capture inaccuracy. These mistakes show up as the iris being tilted toward the corner, the eyes being nearly closed, or an eyelash partially blocking the iris. Handling these difficult situations makes it more difficult to accurately determine Haar features, presenting major challenges that require more research.

The lower accuracy of the current study compared to other studies can be attributed to several factors. First, the variation in image environment conditions, such as lighting, capture distance, and camera resolution, significantly impacts the results. Second, other studies often achieve higher accuracy by testing their methods on a smaller number of datasets comprising high-resolution images, which inherently simplifies the problem and inflates the accuracy. It is crucial to acknowledge that the accuracy of the proposed model is influenced by real Ophthalmologist images, as highlighted in Table 6, to provide a fair assessment of its performance relative to other studies in the field.

Table 6. Accuracy comparisons with related studies.

Study reference	Images (test set)	Method	Dataset	Accuracy (%)
[26]	6	Canny + HT	-	83
[27]	3400	EHT	FERET	97.9
	1521	EHT	BioID	96.4
[28]	94	AFP + FVM	camera	98.9
[29]	150	HT + SF	FaceDB	96.5
[13]	160	HT + CNN	IF3D	98.75
Proposed Method	281	HT + RBFN	IF3D + Other DB	97.5

* HT: Enhanced Hough Transform, CHT: Circular Hough Transform, SF: Separability Filter, FVM: First Valley Method, AFP: Average Feature Point.

Discussion

The proposed method achieved a high overall accuracy of 97.5%. However, it is important to consider certain aspects and limitations of this study. The test set included 281 images, which is larger than most test sets used in similar studies, except for one study [27] that tested on 3,400 images. This difference is largely due to the diverse and challenging nature of the datasets used here. The two datasets, IF3D and the Ophthalmologist dataset were chosen to reflect a wide range of real-world scenarios, all of which increase the datasets complexity.

The recorded lower accuracy of this study compared to others can be attributed to several factors. First, the results are influenced by variations in environmental conditions, such as lighting, capture distance, and camera resolution. Second, many related studies report higher accuracy because they use smaller sets of high-resolution images, which enhance the model learning and inflate accuracy. Additionally, while other studies often utilize deep learning methods that require significantly more training time, the current study adopted a simpler approach using radial basis functions in artificial neural networks. Despite these differences, we believe the accuracy achieved by the proposed model is valuable.

The trade-off between accuracy and robustness is a deliberate design choice. While methods like [28] and [13] achieve slightly higher accuracy, they may not generalize as well to real-world conditions, where variations in image quality can significantly impact performance. In contrast, the proposed approach shows a balanced relation between accuracy and recall with improved computational efficiency; therefore, it is suitable for automatic eye disorder detection.

It also underlines some points of improvement. The proposed method has a relatively lower specificity, which is 33.3%, indicating a limitation in differentiating true negatives effectively. This may be explained by the fact that the datasets are inherently burdened with such variability-occlusions and extreme lighting conditions that make for a difficult learning problem. Advanced regularization techniques and hybrid models in future work can be considered for these limitations to improve specificity.

Furthermore, the robustness of this method to challenging conditions, such as low-resolution images or eye boundaries. In summary, it becomes obvious from these results that strong, generalized algorithms are needed across the spectrum of medical environments, with a critical need for better diagnosis. The proposed approach creates a solid groundwork for integrating computer vision techniques into ophthalmology, hence paving the road for real-time diagnostic tools for considerably improved outcomes.

CONCLUSION

This study tackled one of the big challenges in the field of computer vision in relation with medical field: detecting and classifying types of horizontal eye strabismus. The proposed approach illustrated an effective performance of a six-stages approach which involved image enhancement scheme, detection of the face, and localization of the iris. It drew on two different datasets, such as IF3D and an ophthalmologist dataset, hence covering a wide age group. Iris center position analysis among eye segments proved to be a great added dimension of the study. The evaluation process showcased promising results, with a testing set of 281 images categorized into strabismus types. The method capability to accurately detect and classify these types underlines its potential as a diagnostic tool. The interdisciplinary nature of this research, bridging computer vision and ophthalmology, opens avenues for enhanced ocular health assessment and treatment strategies. As technology advances and datasets expand, the proposed approach lays a strong foundation for further advancements in the field of strabismus detection and diagnosis. It can be used in real-time diagnostics.

SUPPLEMENTARY MATERIAL

None.

AUTHOR CONTRIBUTIONS

Bassam AlKindy: Conceptualization and formal analysis. Oras B. Jamil: Resources and data curation. Huda Al-Nayyef: Methodology and investigation. Wissam Alkendi: Software and validation, writing and editing the original draft preparation.

FUNDING

None.

DATA AVAILABILITY STATEMENT

All data are available in the paper.

ACKNOWLEDGMENTS

The research presented in this paper was supported by Mustansiriyah University (uomustansiriyah.edu.iq), and CIAD lab. for their support in finishing this research study.

CONFLICTS OF INTEREST

The authors declare no conflicts of interest.

REFERENCES

[1] H. Xiao, S. Xiao, G. Ma, and C. Li, "Image Sobel edge extraction algorithm accelerated by OpenCL," *The Journal of Supercomputing*, vol. 78, no. 14, pp. 16 236–16 265, 2022. doi: 10.1007/s11227-022-04404-8.

[2] H. Dhari and N. K. El Abbadi, "Retinal blood vessels segmentation using classical edge detection filters and the watershed," in *2024 25th International Arab Conference on Information Technology (ACIT)*, IEEE, Dec. 2024, pp. 1–7. doi: 10.1109/ACIT62805.2024.10877075.

[3] N. L. Fitriyani, C.-K. Yang, and M. Syafrudin, "Real-time eye state detection system using haar cascade classifier and circular hough transform," in *2016 IEEE 5th Global Conference on Consumer Electronics*, IEEE, Oct. 2016, pp. 1–3. doi: 10.1109/gcce.2016.7800424.

[4] B. J. Maiseli, "Hausdorff distance with outliers and noise resilience capabilities," *SN Computer Science*, vol. 2, no. 5, p. 358, 2021. doi: 10.1007/s42979-021-00737-y.

[5] Y. Qin, H. Lyu, and K. Zhu, "Driver fatigue detection method based on multi-feature empirical fusion model," *Multimedia Tools and Applications*, Aug. 2024. doi: 10.1007/s11042-024-20115-z.

[6] J. A. Nasiri, S. Khanchi, and H. R. Pourreza, "Eye detection algorithm on facial color images," in *2008 Second Asia International Conference on Modelling & Simulation (AMS)*, IEEE, May 2008, pp. 344–349. doi: 10.1109/ams.2008.55.

[7] C. Park, K. Park, and Y. Moon, "Eye detection using eye filter and minimisation of NMF-based reconstruction error in facial image," *Electronics Letters*, vol. 46, no. 2, pp. 130–132, 2010. doi: 10.1049/el.2010.3239.

[8] W. AlKendi, P. Mahapatra, B. Alkindy, C. Guyeux, and M. Barthès, "Application of particle detection methods to solve particle overlapping problems," in *Proceedings of the 3rd International Conference on Image Processing and Vision Engineering*, SCITEPRESS - Science and Technology Publications, 2023, pp. 84–91. doi: 10.5220/0011852500003497.

[9] N. N. Pandey and N. B. Muppalaneni, "Strabismus free gaze detection system for driver's using deep learning technique," *Progress in Artificial Intelligence*, vol. 12, no. 1, pp. 45–59, 2023. doi: 10.1007/s13748-023-00296-8.

[10] P. Viola and M. Jones, "Rapid object detection using a boosted cascade of simple features," in *Proceedings of the 2001 IEEE Computer Society Conference on Computer Vision and Pattern Recognition. CVPR 2001*, ser. CVPR-01, vol. 1, IEEE Comput. Soc, pp. I-511-I–518. doi: 10.1109/cvpr.2001.990517.

[11] G. Zhang, W. Xu, H. Gong, L. Sun, C. Li, H. Chen, and D. Xiang, "Multi-feature fusion-based strabismus detection for children," *IET Image Processing*, vol. 17, no. 5, pp. 1590–1602, 2023. doi: 10.1049/ipr2.12740.

[12] M. Shafi and P. W. H. Chung, "Eyes extraction from facial images using edge density," in *2008 7th IEEE International Conference on Cybernetic Intelligent Systems*, IEEE, Sep. 2008, pp. 1–6. doi: 10.1109/ukricis.2008.4798958.

[13] H. S. Hamid, B. AlKindy, A. H. Abbas, and W. B. Al-Kendi, "An intelligent strabismus detection method based on convolution neural network," *TELKOMNIKA (Telecommunication Computing Electronics and Control)*, vol. 20, no. 6, pp. 1288–1296, 2022. doi: 10.12928/telkomnika.v20i6.24232.

[14] K. Somasundaram and S. Vijayalakshmi, "A novel method for segmentation of the Hippocampus based on watershed algorithm," in *2010 Second International conference on Computing, Communication and Networking Technologies*, IEEE, Jul. 2010, pp. 1–6. doi: 10.1109/icccnt.2010.5591880.

[15] D. C. Prakash, R. C. Narayanan, N. Ganesh, M. Ramachandran, S. Chinnasami, and R. Rajeshwari, "A study on image processing with data analysis," in *Recent Trends in Science and Engineering*, vol. 2393, AIP Publishing, May 2022, p. 020 225. doi: 10.1063/5.0074764.

[16] Y. Yu, H. Huo, and J. Liu, "Facial expression recognition based on multi-channel fusion and lightweight neural network," *Soft Computing*, vol. 27, no. 24, pp. 18 549–18 563, 2023. doi: 10.1007/s00500-023-09199-1.

[17] P. Menezes, J. C. Barreto, and J. Dias, "Face tracking based on haar-like features and eigenfaces," *IFAC Proceedings Volumes*, vol. 37, no. 8, pp. 304–309, 2004. doi: 10.1016/s1474-6670(17)31993-6.

[18] J. Barreto, P. Menezes, and J. Dias, "Human-robot interaction based on Haar-like features and eigenfaces," in *IEEE International Conference on Robotics and Automation, 2004. Proceedings. ICRA'04. 2004*, IEEE, Sep. 2004, 1888–1893 Vol.2. doi: 10.1109/robot.2004.1308099.

[19] A. M. El-Helw, M. A. Sharkas, and E. I. AlSaba, "Combing Haar and MBLBP features for face detection using multi-exit asymmetric boosting," in *2010 2nd International Conference on Software Technology and Engineering*, IEEE, Oct. 2010. doi: 10.1109/icste.2010.5608764.

[20] P. Verma, K. Verma, A. Singh, A. K. Sundaram, and V. S. Bramhe, "Real-Time vehicle detection and tracking system using cascade classifier and background subtractor," in *Computer Vision and Robotics*. Springer Nature Singapore, Apr. 2023, pp. 431–441. doi: 10.1007/978-981-19-7892-0_34.

[21] J.-c. Chen, P.-q. Yu, C.-y. Yao, L.-p. Zhao, and Y.-y. Qiao, "Eye detection and coarse localization of pupil for video-based eye tracking systems," *Expert Systems with Applications*, vol. 236, p. 121 316, Feb. 2024. doi: 10.1016/j.eswa.2023.121316.

[22] S. Umer and B. C. Dhara, "A fast iris localization using inversion transform and restricted circular Hough transform," in *2015 Eighth International Conference on Advances in Pattern Recognition (ICAPR)*, IEEE, Jan. 2015, pp. 1–6. doi: 10.1109/icapr.2015.7050667.

[23] S. K. Vasudevan, A. Baskar, M. Rajappa, and T. S. Murugesh, *Digital image processing*. Chapman and Hall/CRC, Apr. 2023. doi: 10.1201/9781003217428.

[24] S. E. Umbaugh, *Digital image processing and analysis: Computer vision and image analysis*. CRC Press, Nov. 2022. doi: 10.1201/9781003221135.

[25] C. T. Nakas, L. E. Bantis, and C. A. Gatsonis, *ROC analysis for classification and prediction in practice*. Chapman and Hall/CRC, May 2023. doi: 10.1201/9780429170140.

[26] D. Ali and A. Das, "Face detection and eye extraction using Canny edge detection and Hough transform," in *Proceedings of conference on Advancement in Computation, Communication and Electronics Paradigm (ACCEP-2019)*, Jan. 2019, pp. 14–18. [Online]. Available: https://www.vidyamandira.ac.in/pdfs/publications/seminar_Proceeding/cs_conference_accep_2019.pdf#page=20.

[27] T. Fawcett, "An introduction to ROC analysis," *Pattern Recognition Letters*, vol. 27, no. 8, pp. 861–874, 2006. doi: 10.1016/j.patrec.2005.10.010.

[28] F. Yang, Y. Dai, L. Wang, and Z. Jia, "The iris feature point averaging method in student eye gaze tracking," in *2018 37th Chinese Control Conference (CCC)*, IEEE, Jul. 2018, pp. 5520–5524. doi: 10.23919/chicc.2018.8482573.

[29] T. Kawaguchi, D. Hidaka, and M. Rizon, "Detection of eyes from human faces by Hough transform and separability filter," in *Proceedings 2000 International Conference on Image Processing (Cat. No.00CH37101)*, ser. ICIP-00, vol. 1, IEEE, Aug. 2002, pp. 49–52. doi: 10.1109/icip.2000.900889.